Project Acronym:

FUSVET (SEED/1221/0080)

Focused Ultrasound System for veterinary chemotherapeutic applications for oncology

Deliverable number: 3.2

Title: MRI compatible ultrasonic transducer

Prepared by:

Nikolas Evripidou (CUT)
Anastasia Antoniou (CUT)
Christakis Damianou (CUT)

Date: 15/09/2023

Ευρωπαϊκή Ένωση
Ευρωπαϊκά Διαρθρωτικά και Επενδυτικά Ταμεία

Κυπριακή Δημοκρατία

Διαρθρωτικά Ταμεία της Ευρωπαϊκής Ένωσης στην Κύπρο

Table of Contents

Executive summary

The current deliverable presents the procedure that was followed for the development of the transducers to be incorporated in the FUSVET robotic system. Initially, a MATLAB-based software was utilized for simulating the high intensity focused ultrasound (HIFU) beams and the heating effects of candidate transducers to determine the most suitable one for the intended application of FUSVET. A transducer with a relatively high frequency of 2.75 MHz, 50-mm diameter, and 65-mm radius of curvature was manufactured for precisely targeting shallow tissue. Another transducer with a frequency of 1 MHz, a diameter of 90 mm and a radius of curvature of 100 mm was deemed suitable and selected for manufacturing, so that deeper tissue can be reached as well. Overall, these transducers were chosen on the criterion of achieving strong focusing of ultrasound (US) waves over a large depth.

In each case, a dedicated transducer housing was designed, and 3D printed using Acrylonitrile styrene acrylate (ASA) plastic to host the transducer element. The top and bottom conductive surfaces of the element were connected to a coaxial cable to create the electric circuit required for activating the transducer. The bottom of the housing was sealed with a perforated plastic cover for better cooling of the transducer when operating in a liquid environment. The housing was filled with epoxy that serves as the backing material, providing electrical isolation and preventing potential damage of the electric circuit. When operating in the MR environment, the transducer is connected to a low-pass RF filter for preventing image distortions effects.

Each transducer was tuned to a 50 Ω impedance. A matching network was designed and incorporated between the amplifier and the transducer to achieve proper impedance matching at the frequencies of interest. Specifically, a circuit of inductors and capacitors was designed to adjust the input impedance of the transducer so as to maximize the power transfer from the amplifier to the transducer. The suitable electrical parameters of the circuit components were determined by Smith chart calculations.

Safe operation of the transducer in the MRI environment is required for proper image acquisition and real-time monitoring of the ablation procedure. Therefore, the selection of transducer materials was based on MRI compatibility. The transducer was made of a piezoceramic element accommodated in a housing made of ASA plastic and covered with epoxy, of which all are considered to be MR compatible. Regarding the electric circuit, non-ferromagnetic metals were utilized for its construction.

After construction, the transducers were evaluated for their acoustic efficiency according to the radiation force balance method, utilizing a power meter. Hydrophone measurements were also performed to evaluate the actual ultrasonic field distribution. The axial pressure profiles provided information about the actual location and size of the focal spot. Moreover, evaluation of the generated ultrasonic fields was done by sonicating transparent plastic films. The effect of the distance of each transducer from the plastic film on lesion formation was examined.

Evaluation of the transducers' functionality and compatibility with a high-field MRI scanner is the subject of Del. 3.4.

Results

HIFU beam simulations

Simulations of the ultrasonic field of the candidate transducers were performed_utilizing the open source software "HITU simulator", written by Joshua Soneson [1]. Regarding the structural characteristics of the spherical transducers, several combinations of the frequency, diameter (D) and radius of curvature (R) were tested. A frequency of 2.75 MHz suitable for shallow targets was tested using D = 40-60 mm and R = 50-70 mm. HIFU beams of lower frequency of 1 MHz suitable for deeper targets were simulated for D = 70-90 mm and R = 80-100 mm. Natural characteristics of the HIFU beams, as well as their heating effects in layered media, were predicted by the software. The output was released to the MATLAB workspace in the form of graphs for further analysis.

These simulations aided the selection of the optimal transducer elements. The one with a high central frequency of 2.75 MHz, a diameter of 50 mm and a radius of curvature of 65 mm was chosen because it offered strong focusing, which is required for precise targeting of shallow tumors. For the lower operating frequency of 1 MHz, a diameter of 90 mm and a radius of curvature of 100 mm were selected. These structural characteristics resulted in a strongly focused beam. Furthermore, the larger radius of curvature will allow targeting deeper-seated tumors. Moreover, both simulated beams resulted in a very good lesion length to diameter ratio.

Indicative simulation results for the selected transducers using an acoustical power of 60 W for 30 s are listed in Table 1. The half intensity width (full width half maximum (FWHM) of the radial US intensity profile) and the half intensity length (FWHM of the axial intensity profile) as estimated utilizing the tools provided by MATLAB are indicative of the expected focal point dimensions. The expected ratio of lesion length to diameter is also listed in this table.

Table 1: The characteristics of the selected transducers and indicative simulation results.

Frequency (MHz)	Diameter (mm)	Radius of curvature (mm)	Half intensity width (mm)	Half intensity length (mm)	Ratio of lesion length to diameter
1	90	100	1.6	10.5	6.56
2.75	50	65	0.60	4.94	8.23

The simulation results for both transducers, including graphs of the axial and radial distribution of the HIFU field, the temperature distribution, and thermal dose accumulation, are next presented. The parameters of the bioheat equation and the arrangement of materials used in each simulation are also provided.

The beam propagation was simulated in the layered media as shown in Figure 1. The blue areas represent water, which served as a coupling media for effective ultrasound transmission, while the middle red area represents a 4-cm thick tissue. The transducer element is represented by the red line at the left side. Accurate soft tissue simulation was achieved by introducing the acoustic and thermal properties of an agar-based tissue mimicking phantom. The radius of curvature of the two selected transducers with frequencies of 2.75 and 1 MHz is 6.5 and 10 cm,

respectively. For both transducer the focal point was set at 2 cm within the tissue. Therefore, the distance between the surface of the two transducers and the tissue was 4.5 and 8 cm, respectively. The bioheat parameters used to run the simulations are listed in Table 2.

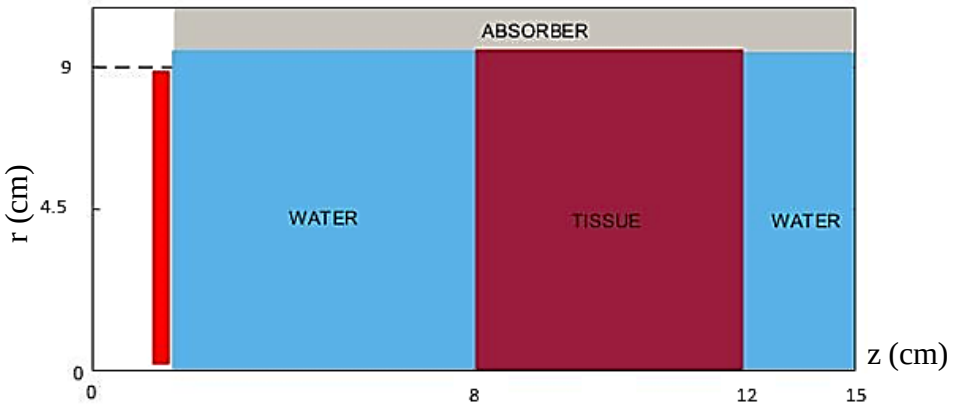

Figure 1: Materials arrangement used in the simulation (1 MHz transducer with radius of curvature of 10 cm; focal depth of 2 cm).

Table 2: Parameters for the bioheat equation.

Parameter	Variable	Value	Unit
Sonication duration	t_h	30	s
Cooling duration	t_c	30	s
Baseline temperature	Teq	31	ºC
Dose threshold for safety	safety	80	CEM_{43}
Dose threshold for efficacy	efficacy	240	CEM_{43}

Table 3 lists all the parameters used for the HIFU field simulation, including the transducers specifications, the computational parameters, as well as the acoustic and thermal properties of the layered media.

Table 3: Set-up parameters used for the HIFU field simulation.

	Parameter	Variable	Value	Unit
Transducer	Frequency	Tx.f	**1.0e6 / 2.75e6**	Hz
	Inner radius	a_1	0	cm
	Outer radius	a_2	**4.5 / 2.5**	cm
	Focusing depth	Tx.d	**10 / 6.5**	cm
	Power	Tx.P	60	W
Computational domain	Starting point	z_start	$d - \sqrt{d^2 - a_2^2}$	cm
	Max axial distance	Grid.Z	15 / 11.5	cm
	Number of harmonics	Grid.KK	128	-
	Radial grid density	ppw_r	15	-
	Axial grid density	ppw_z	10	-
Hydrophone	Element diameter	hd	0.2	mm

Graphical output	Axial locations	z_output	9.778 / 6.302	cm
Material	Number of layers	II	3	-
Material 1	Material transition distance	Layer(1).z	0	cm
	Small-signal sound speed	Layer(1).c	1482	m/s
	Mass density	Layer(1).rho	1000	Kg/m^3
	Attenuation at 1 MHz	Layer(1).alpha	15	dB/m
	Fraction due to absorption	Layer(1).fraction	0	-
	Exponent of attenuation power law	Layer(1).eta	2	-
	Nonlinear parameter	Layer(1).beta	3.5	-
	Heat capacity	Layer(1).Cp	4180	J/kg/K
	Thermal conductivity	Layer(1).kappa	0.6	W/m/K
	Perfusion rate	Layer(1).w	0	$Kg/m^3/s$
Material 2	Material transition distance	Layer(2).z	**8 / 4.5**	cm
	Small-signal sound speed	Layer(2).c	1629	m/s
	Mass density	Layer(2).rho	1000	Kg/m^3
	Attenuation at 1 MHz	Layer(2).alpha	10	dB/m
	Fraction due to absorption	Layer(2).fraction	0.9	-
	Exponent of attenuation power law	Layer(2).eta	1	-
	Nonlinear parameter	Layer(2).beta	4.5	-
	Heat capacity	Layer(2).Cp	4180	J/kg/K
	Thermal conductivity	Layer(2).kappa	0.6	W/m/K
	Perfusion rate	Layer(2).w	20	$Kg/m^3/s$
Material 3	Material transition distance	Layer(3).z	**12 / 8.5**	cm
	Small-signal sound speed	Layer(3).c	1482	m/s
	Mass density	Layer(3).rho	1000	Kg/m^3
	Attenuation at 1 MHz	Layer(3).alpha	15	dB/m
	Fraction due to absorption	Layer(3).fraction	0	-
	Exponent of attenuation power law	Layer(3).eta	2	-
	Nonlinear parameter	Layer(3).beta	3.5	-
	Heat capacity	Layer(3).Cp	4180	J/kg/K
	Thermal conductivity	Layer(3).kappa	0.6	W/m/K
	Perfusion rate	Layer(3).w	0	$Kg/m^3/s$

Quantitative data was generated from the simulation on the acoustic pressure and intensity distribution, the temperature distribution and the corresponding thermal dose accumulation in axial plane, as well as the temporal distribution of temperature at the focal point. The corresponding plots for the 1 MHz transducer are shown in following

Figure 2 to Figure 7.

The axial distribution of pressure of the first five harmonics is shown in Figure 2A. The peak pressure of the first harmonic is 6.5 MPa. The corresponding intensity graph for the first harmonic is shown in the Figure 2B. The corresponding peak intensity of the first harmonic is 1375 W/cm^2. According to the graph, the maximum intensity occurs at 9.77 cm from the surface of the transducer, and thus, the simulated focal depth is 1.77 cm.

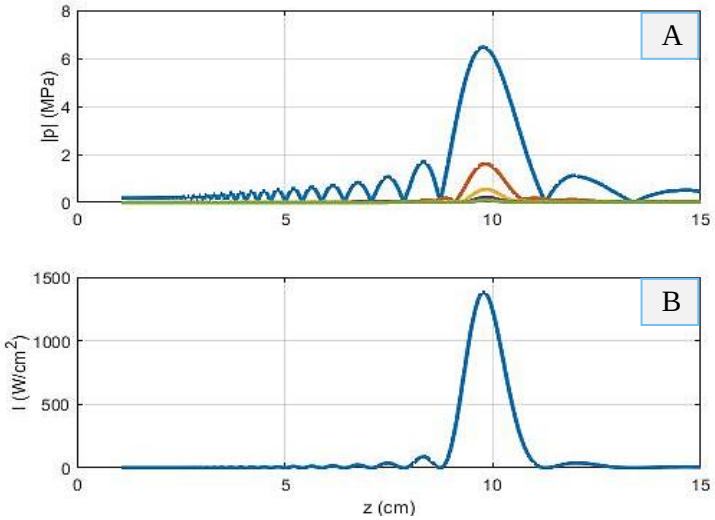

Figure 2: Axial distribution of the (A) first five harmonic pressure amplitudes and (B) intensity for the first harmonic (1 MHz transducer).

The focal distance of 9.77 cm, at which the intensity of the first harmonic was maximum, was used to find the radial pressure distribution. The plots of the first five harmonic pressure amplitudes are shown in Figure 3A. Figure 3B shows the intensity of the first harmonic plotted against the radial distance from the axis of the transducer. The pressure at the central axis of the beam peaked at approximately 6.5 MPa, whereas the corresponding acoustic intensity was found to be around 1400 W/cm^2. The simulated axial power profile (

Figure 2) indicates a half intensity length of 10.5 mm while the radial power profile (Figure 3) shows a half intensity width of 1.6 mm.

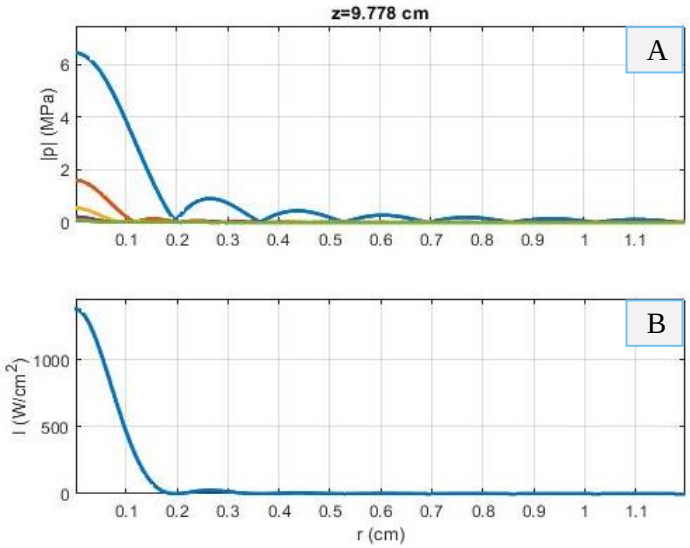

Figure 3: Radial distribution of the (A) first five harmonic pressure amplitudes and (B) intensity for the first harmonic at Z = 9.778 cm (1 MHz transducer).

The shape and size of the focal spot were approximated by the software. The qualitative plot of the ultrasonic spatial distribution on the axial plane, for a maximum axial distance (z) of 15

cm from the surface of the transducer is illustrated in following Figure 4. The vertical scale (r) indicates the diameter of the beam at each sonication depth (z).

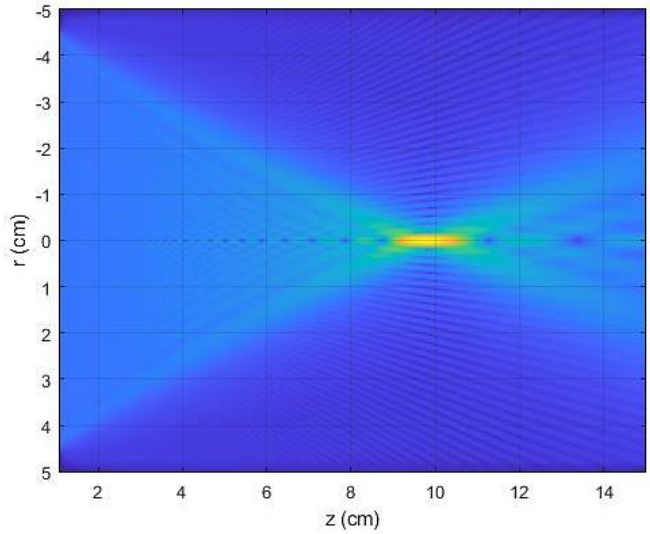

Figure 4: A qualitative plot of the spatial distribution of the ultrasound field.

Figure 5 shows the temperature profile extracted using an acoustic power of 60 W for a sonication time of 30 s at a focal depth of 1.77 cm. During the 30 s sonication, heat absorption is responsible for the temperature rise, while conduction decreases the rate of temperature elevation. Post-sonication (30-60 s) only conduction mechanism remains, resulting in temperature reduction. According to the graph, the maximum temperature reached was 64.3 ^{o}C. A temperature increase of 33.3 ^{o}C from the baseline temperature of 31 ^{o}C was sufficient to create thermal lesion.

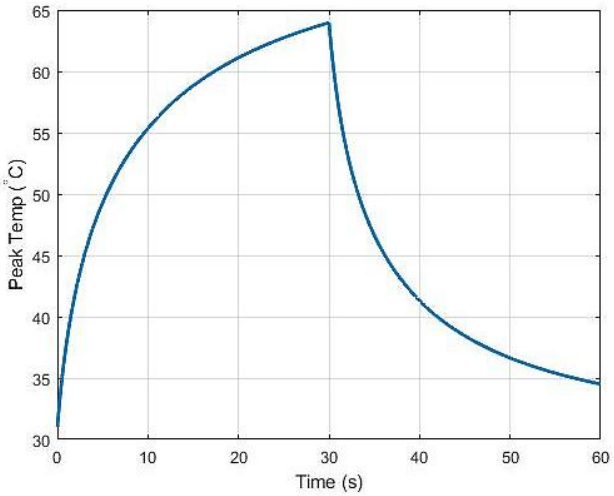

Figure 5: Peak temperature versus time during and after sonication at 60 W (1 MHz transducer).

The peak temperature occurs at 30 s where the sonication is completed. Figure 6 shows the spatial distribution of the temperature at this time point. The approximate size of the created lesion can be estimated from the temperature distribution map. Since the ablation is performed when the tissue is heated to 60 ^{o}C and above, the calculated temperatures indicate a lesion of 8.2 mm in length and 1.6 mm in diameter.

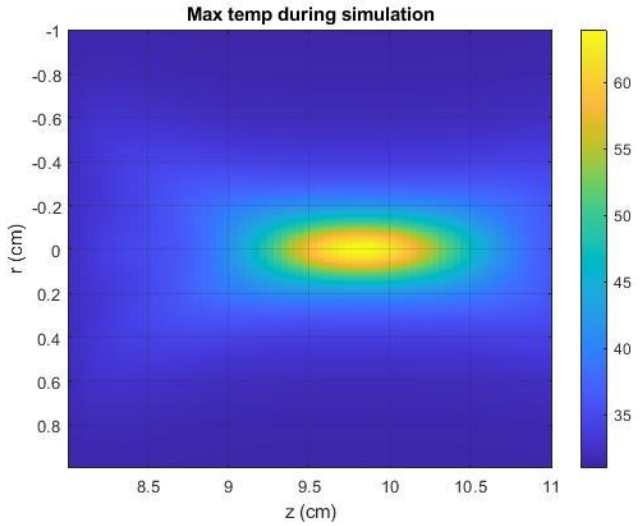

Figure 6: Temperature distribution (axial plane) at the time peak temperature occurs (1 MHz transducer).

Furthermore, the pressure distribution was used to calculate the thermal dose according to the defined treatment protocol. Figure 7 shows the thermal dose accumulation. Two curves are shown; one at 80 CEM and one at 240 CEM (defined as cumulative equivalent minutes). The first one indicates the region where no significant thermal effects occur while the later one shows the region of total necrosis. When the thermal dose is equal or larger than 240 CEM, tissue necrosis occurs. Thereby, the yellow line is the threshold that defines the (enclosed) area of necrosis.

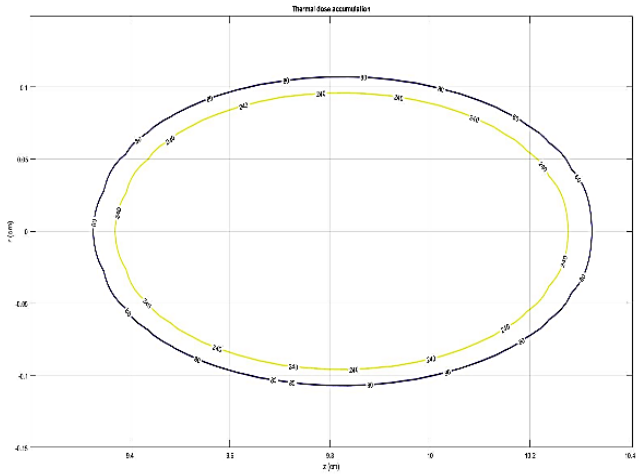

Figure 7: Thermal dose calculation (1 MHz transducer).

Based on the estimated thermal dose, the simulated lesion length and diameter are approximately 9 mm and 1.8 mm, respectively. Note that these values match well those estimated by the temperature map of Figure 6.

The corresponding simulation plots for the 2.75 MHz transducer are shown in following Figure 8 to Figure 13.

The axial pressure distribution of the first five harmonics is shown in Figure 8A, with a peak pressure of 9.11 MPa, while Figure 8

Figure 2B shows the corresponding intensity graph of the first harmonic with a peak value of 3693 W/cm^2. According to the graph, the maximum intensity occurs at a distance of 6.302 cm from the surface of the transducer, therefore the focal depth is 1.802 cm. Accordingly, the radial pressure distribution was calculated at the focal distance of 6.302 cm. The plots of pressure distribution for the first five harmonics are shown in Figure 9Figure 3A, whereas Figure 9B shows the intensity of the first harmonic as a function of radial distance from the axis of the transducer. The simulated axial power profile (Figure 8) indicates a half intensity length of 4.94 mm while the radial power profile (Figure 9) reveals a half intensity width of 0.60 mm.

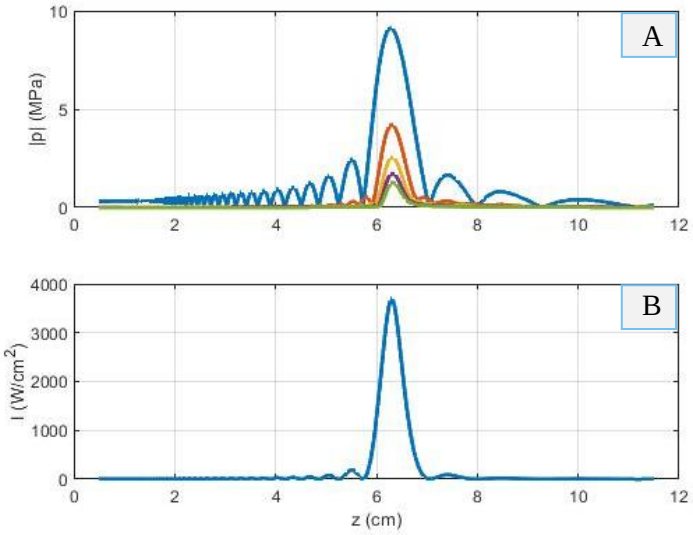

Figure 8: The axial distribution of the (A) first five harmonic pressure amplitudes and (B) intensity for the first harmonic (2.75 MHz transducer).

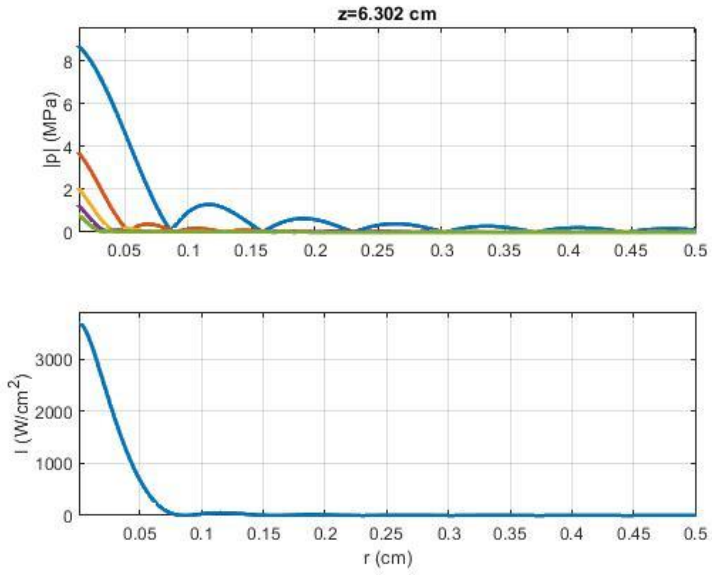

Figure 9: Radial distribution of the (A) first five harmonic pressure amplitudes and (B) intensity for the first harmonic at Z = 6.302 cm (2.75 MHz transducer).

The spatial distribution of the ultrasound beam for a maximum axial distance (z) of 11.5 cm, is shown in the qualitative diagram of Figure 10. The vertical axis (r) shows the beam diameter for each sonication depth (z).

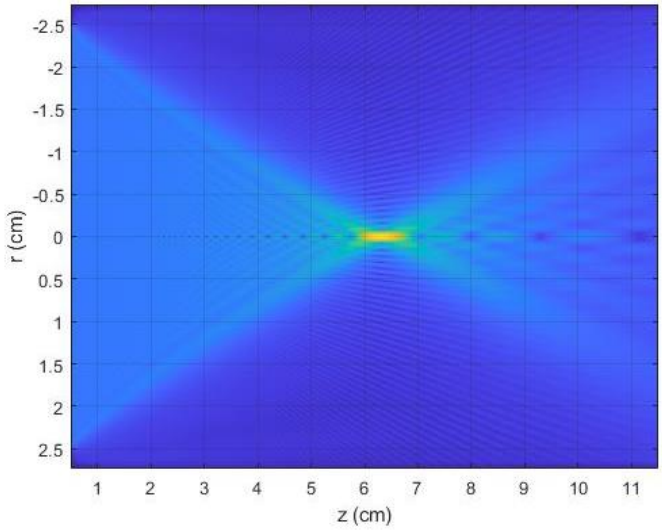

Figure 10: A qualitative plot of the spatial distribution of the ultrasound field (axial plane).

The maximum temperature reached using acoustic power of 60 W for 30 s was extracted from the temperature profile of Figure 11 and had a value of 130.8 °C. The temperature profile was acquired at a focal depth of 1.802 cm. The spatial distribution of the temperature at 30 s (where temperature is maximized) is presented in Figure 12.

The corresponding thermal dose accumulation, which defines the size of the lesion, is shown in Figure 13. Tissue necrosis occurs when the thermal dose is equal to or greater than 240 CEM. Therefore, the lesion formed is expected to have dimensions of approximately 11.7 mm in length and 3.2 mm in width.

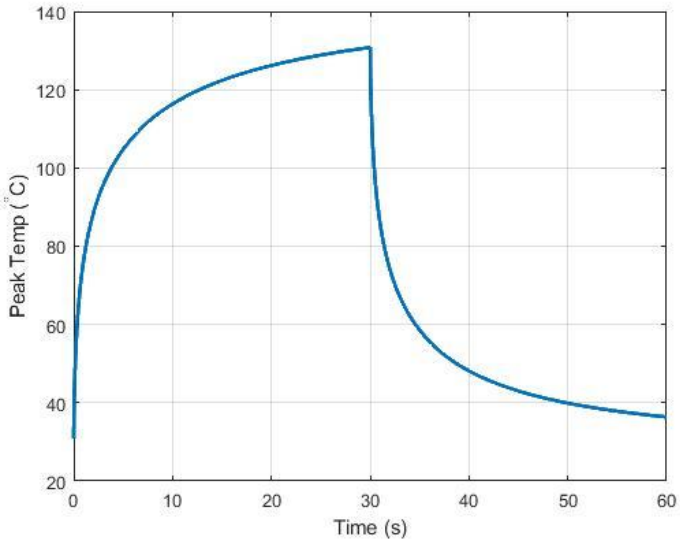

Figure 11: Focal temperature versus time for a 30 s sonication at 60 W (2.75 MHz transducer).

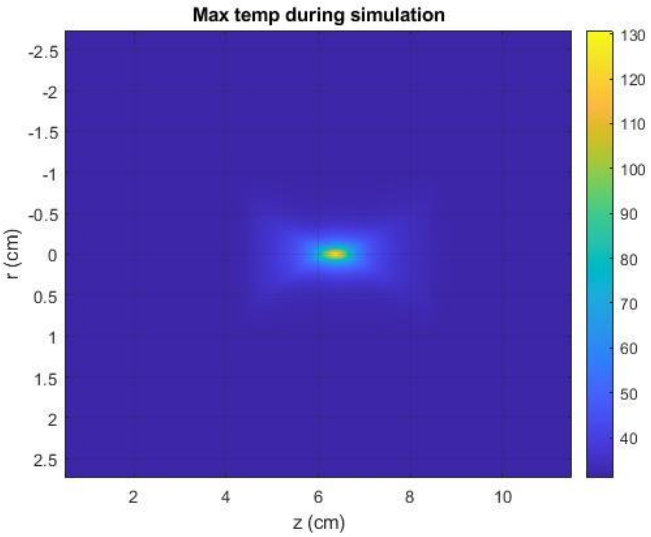

Figure 12: Temperature distribution (axial plane) at the time peak temperature occurs (2.75 MHz transducer).

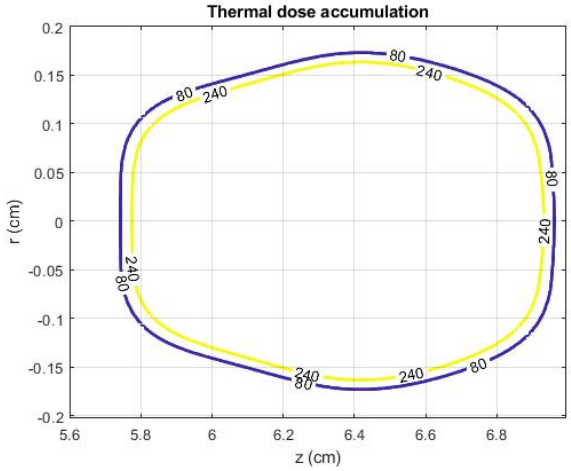

Figure 13: Thermal dose calculation (2.75 MHz transducer).

Transducer Design

The transducers were specially designed to be single element, spherically focused, and compact. Purchased piezoelectric elements were housed in plastic cases and covered by an encapsulant. Ultrasonic transducer elements made out of P762-type piezoceramic, with the selected specifications of a) central frequency of 1 MHz, 90-mm diameter, and 100-mm radius of curvature, and b) central frequency of 2.75 MHz, 50-mm diameter, and 65-mm radius of curvature, were provided by the Piezo Hannas (Wuhan, China) company. The manufacturing process of the transducers is next described. Special emphasis was placed on the selection of the suitable materials to achieve long-term high-power operation of the transducers.

A housing was initially manufactured on a 3D printer (STRATASYS, F270, Eden Prairie, Minnesota, USA) [2] using ASA plastic. This thermoplastic material has good mechanical

properties and high service temperature, and it is MRI compatible. High-temperature tolerance is required so that the housing resists thermal degradation and maintains sufficient strength during continuous sonications. The housing includes a ring-shaped structure wherein the element was soldered. Figure 14 shows a CAD drawing of the ring-shaped structure. The top side was slightly extended radially towards the center to create a lip for supporting the element, as shown in Figure 14B. A step was also designed at the bottom side to enable attachment of the rear cover of the transducer.

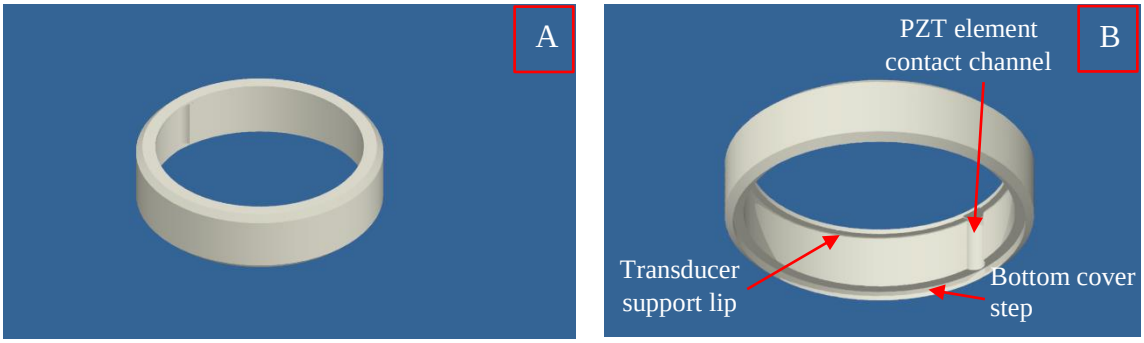

Figure 14: Ring-shaped structure of transducer housing, A) top view, B) bottom view.

Next, a contact was placed on each side (left and right) of the element, as shown in Figure 15. Some constraints were faced during the soldering procedure due to the nature of the piezoelectric element, which is actually a piezoceramic layer covered by screen-printed silver electrodes. The first challenge relates to the soldering time since if it exceeds 2-3 s the electrode may be dissolved in the solder. The soldering temperature is also crucial. If the piezoelectric material is heated to its curie point the domains will become disordered, and the material will be depolarized. Thereby, the soldering iron was set within the temperature range of 250-300^{o}C, as per manufacturer instructions. Furthermore, a specific type of solder was selected, which contained 3% weight per volume (w/v) silver in order to increase the soldering time. Following soldering of the contacts, the element was fixed within the ring-shaped structure of the transducer housing and secured using a thin layer of epoxy that was spread along the perimeter of the housing, as shown in Figure 15B.

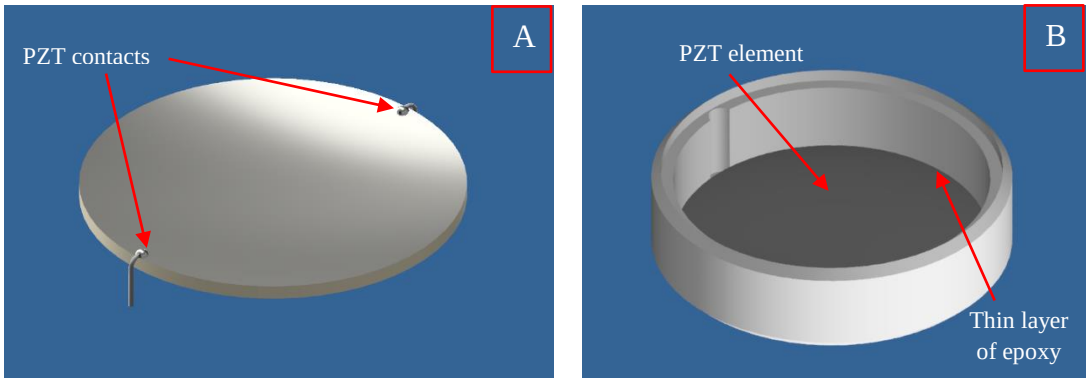

Figure 15: A) Ultrasonic element with the contacts soldered on the top surface. B) The transducer element glued in the ring-shaped structure with a thin layer of epoxy.

The two front contacts were connected to the central conductor of the coaxial cable, whereas the outer conductor was divided into three thinner conductors, which were soldered on the bottom electrode, as shown in

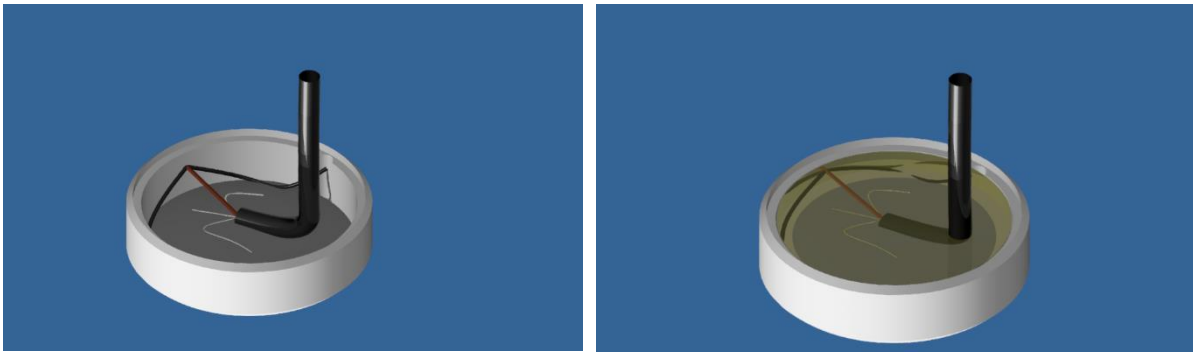

Figure 16A. The specific configuration ensures that in case of a contact failure the transducer will continue operating. With the completion of the electric circuit, the contacts were encapsulated with epoxy, as shown in

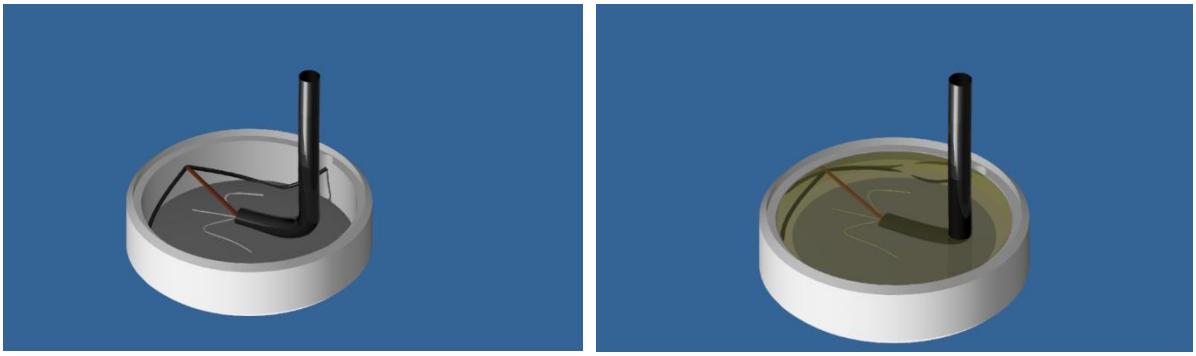

Figure 16B. Epoxy serves as the backing material that isolates the contacts and prevents excessive vibration of the piezoelectric element whilst improving the acoustic performance of the transducer. A two-component epoxy adhesive (ASonic, Tržaška c. 134, 1000 Ljubljana, Slovenia) that can withstand temperatures higher than these typically produced during long-term sonications was selected to ensure a safe and stable performance of the transducer.

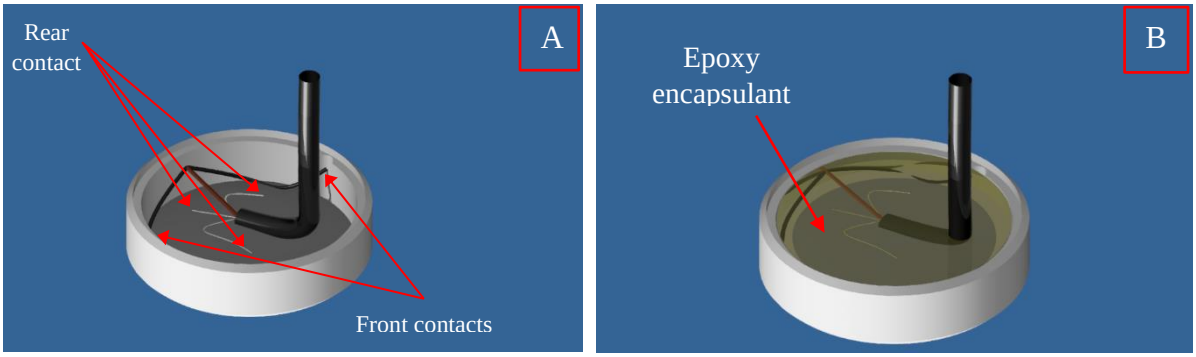

Figure 16: A) The contacts soldered to the coaxial cable. B) The contacts encapsulated with epoxy.

Figure 17 shows a CAD drawing of the designed transducer. Figure 17B shows the plastic cover that sealed the bottom of the ring-shaped structure, thus completing the housing assembly. The plastic cover was specially designed to cover the epoxy layer and improve the

transducer aesthetically whilst allowing cooling of the transducer during operation in a water environment through the hexagonal holes shown in Figure 17B. The coaxial cable was advanced through a dedicated hole of the back cover of the housing, as shown in Figure 17B.

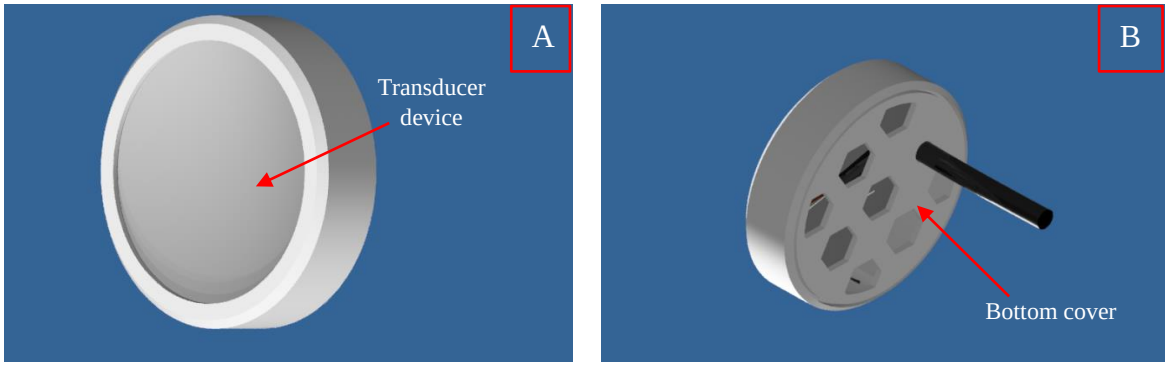

Figure 17: CAD drawing of the transducer, A) top view), B) bottom view.

In the MRI setting, the transducer is connected to an extension cable via an SMA connector to enable connection with the amplifier located outside of the MRI room. A low-pass RF filter (L8959, Anatech electronics, Manhattan, USA) [3] is also incorporated to cut off signals with frequencies higher than 10 MHz and prevent image distortion phenomena.

The selection of transducers' materials was based on MRI compatibility. The transducer elements are made out of piezoceramic material, which is non-magnetic, and thus suitable for use in the MRI environment. The element housings were made of ASA plastic, which is a non-magnetic material as well. Furthermore, a metal-free epoxy was used as the backing material. Regarding the electric circuit, the contacts were made from aluminum (non-ferromagnetic material) strings, and the central conductor was made from copper, which is considered MRI compatible when used in proper amount. Notably, the MRI compatibility of the manufactured transducers will be evaluated inside a strong magnetic field scanner in the framework of Task 3.5 (Del. 3.4). Indicative photos of the developed transducers are shown in Figure 18.

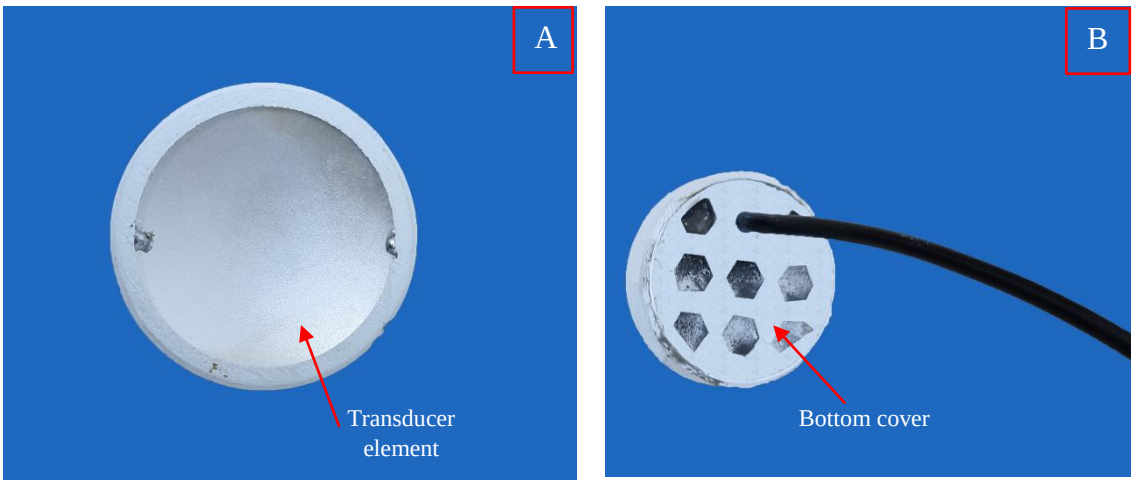

Figure 18: Photo of the developed transducer, A) top view, B) bottom view.

Transducer matching network

The 1 MHz transducer needed a matching network to operate properly. The optimization of the transducer's power output and complementary increase in efficiency was achieved by creating a matching network to maximize the power transfer from the amplifier to the transducer. A circuit of inductors and capacitors was created and incorporated between the amplifier and the ultrasound source so that the resistance of the transducer is equal to the internal resistant of the amplifier.

The transducer was initially connected to the 50 Ω port of the vector network analyzer (MS2026C, Anristsu, Atsugi, Kanagawa Prefecture, Japan) to measure its resistance, as illustrated in Figure 19. A Smith chart was used for impedance matching, according to which the normalized load impedance can be defined as $Z = r + ix$. The estimated transducer impedance at the frequency of 1.097 MHz was Z = 103.660 - 80.789 i. This value was extracted from the Smith chart shown in Figure 20.

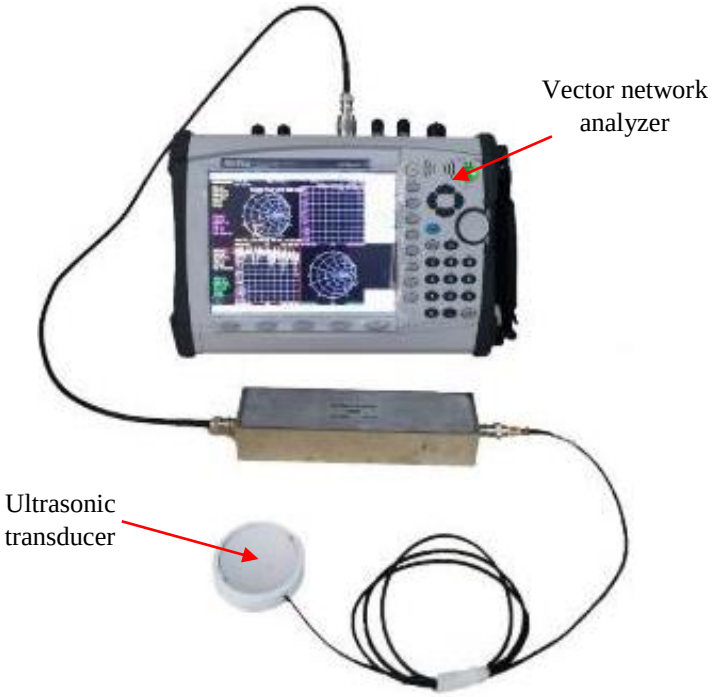

Figure 19: Transducer's impedance measurement without the matching network.

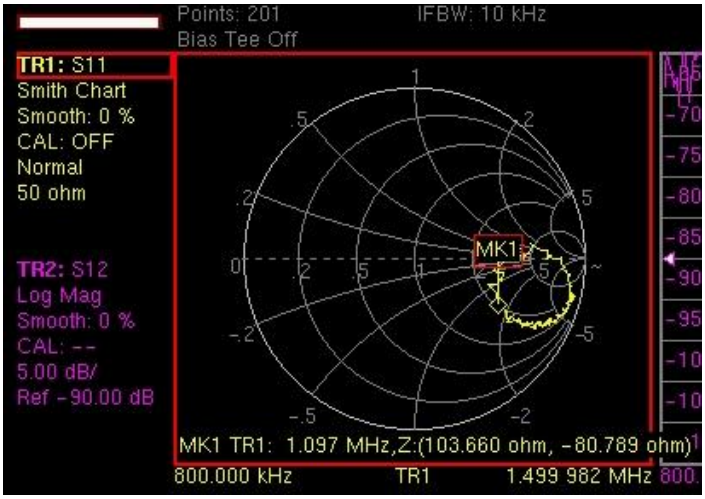

Figure 20: Smith chart of the transducer without the matching network.

The matching network parameters were calculated by an online tool from the website "Leleivre.com" [4]. The circuit options offered by the website are shown in Figure 21. Based on the results, the first circuit was designed having a capacitor of 697.0 pF in parallel with the transducer and an inductor of 11.12 µH in series with the source. An LCR meter (3532-50 LCR Hitester, Hioki, Nagano Prefecture, Japan) was used to find the capacitor with a capacitance value closest to the desired one.

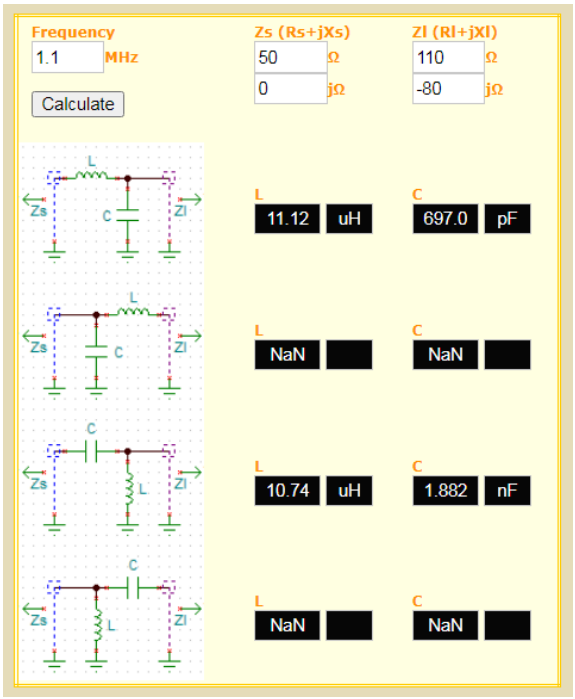

Figure 21: Le leivre online matching network designer.

A second website called "coil32.net" [5] was used to calculate the number of turns the coil needed. The results window of the "coil32.net" website is shown in Figure 22. Based on the

results, a wire with a length of about 2.296 m was utilized to create a double-layer coil, with 42 turns of winding and a winding thickness of 2.18 mm.

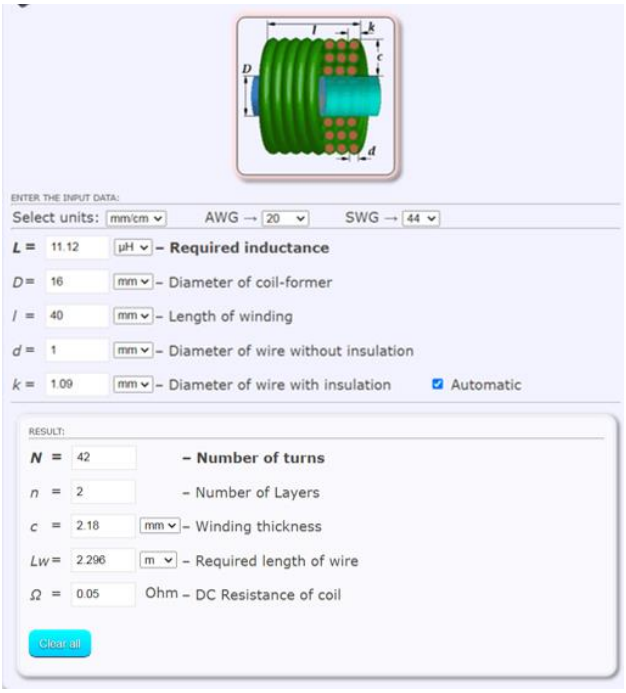

Figure 22: Coil32 online coils design calculator

After the necessary circuit characteristics were determined, the matching network was assembled in an aluminum housing, as shown in Figure 23.

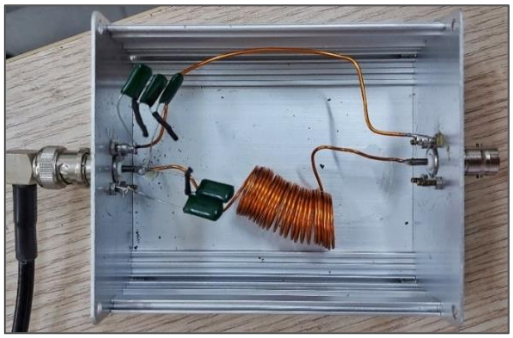

Figure 23: The developed matching network (view of interior).

The impedance of the transducer was then measured with the matching device incorporated in the circuit. However, the impedance did not match the desired value. This was attributed to the fact that the addition of the aluminum enclosure affected the induced electromagnetic field of the coil. Thereby, the circuit components were properly modified to achieve the desired value of impedance. The final values of electrical capacitance and coil turns are listed in Table 4.

Finally, the matching device was connected in series with the transducer and the impedance was measured utilizing the vector network analyzer, in order to assess whether a proper impedance matching was achieved. The corresponding set-up is illustrated in Figure 24. The

final measurement of the transducer impedance with the matching network was Z=49.985 - 2.592i at a frequency of 1.139 MHz. This value was extracted from the Smith chart shown in Figure 25.

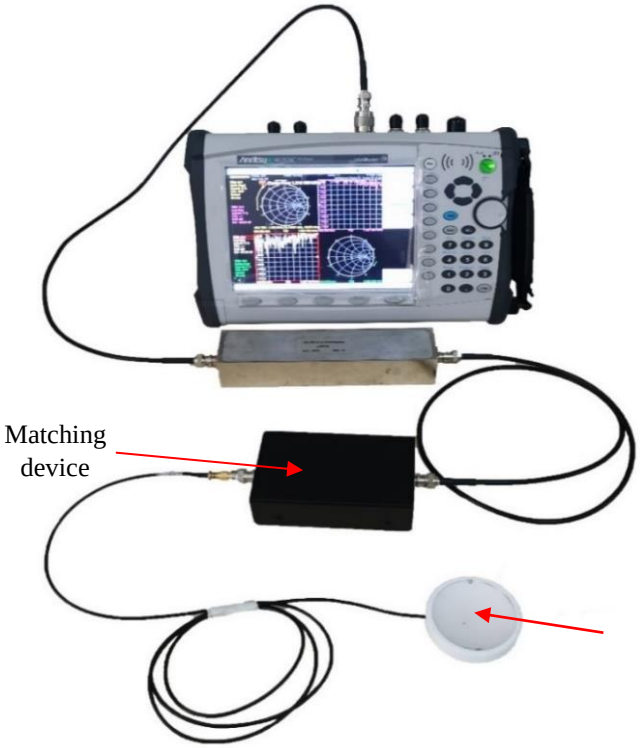

Figure 24: Transducer's impedance measurement with the matching network

Table 4: The electrical capacitance and coil turns of the developed matching network.

Component	Value
Coil turns	21
Capacitor	4.8 nF

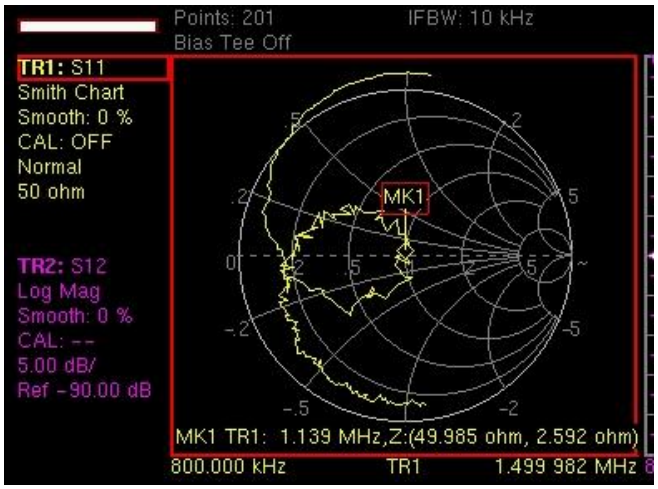

Figure 25: Smith chart of the transducer with the matching network.

Transducer efficiency

The radiation force balance method was employed to calculate the efficiency of the designed transducers using an ultrasonic power meter (UPM-DT100N, Ohmic instruments co, St. Charles, MO 63301, USA) with a measurement range of 0 to 30 W. An RF amplifier (AG1012, AG Series Amplifier, T & C Power Conversion, Inc., Rochester, US) was connected to the transducer, which was placed above a cone-shaped sensor of the power meter in a water media, as shown in Figure 26. The sensor was connected to a precision balance. When acoustic power was applied, the resultant force exerted on the cone was directly proportional to the total radiated power. The position of the ultrasonic transducer was adjusted by a movable holder. For each applied electric power, the position of the transducer was adjusted until the maximum acoustic power was measured. This way it was ensured that the total acoustic power produced was measured by the power meter.

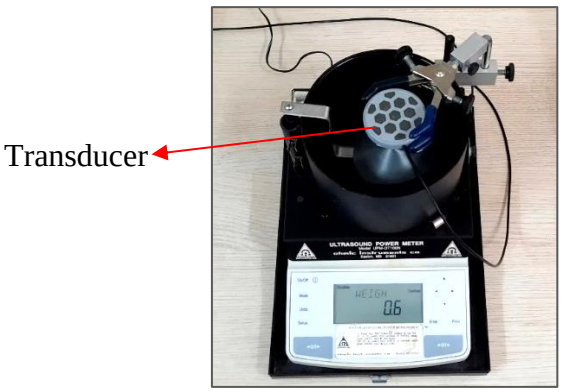

Figure 26: Photo of the power meter used for measuring the acoustic power of the transducers.

1 MHz Transducer

A range of electrical powers from 1 - 30 W was applied to calculate the transducer's efficiency. Table 5 lists the electrical power values and corresponding acoustic power values.

Table 5: The electrical power applied, and acoustic power produced.

Electric Power (W)	Acoustic Power (W)
1	0.8
2	1.0
5	1.8
10	3.0
15	4.2
20	5.7
30	8.2

The transducer's efficiency indicates the percentage of electric power (input) converted to acoustic power (output) and was calculated by equation [1] using the data of Table 5:

$$Efficiency = \frac{Acoustic\ power}{Electric\ power}\ x\ 100\% = \frac{8.2\ W - 0.8\ W}{30\ W - 1\ W}.100\% = 25.52\% \qquad [1]$$

For more accurate calculation of efficiency, the measured acoustic power was plotted as a function of the applied electrical power, as shown in Figure 27. The slope of the graph was calculated by linear regression adjustment. The estimated value of the efficiency was 25.8%.

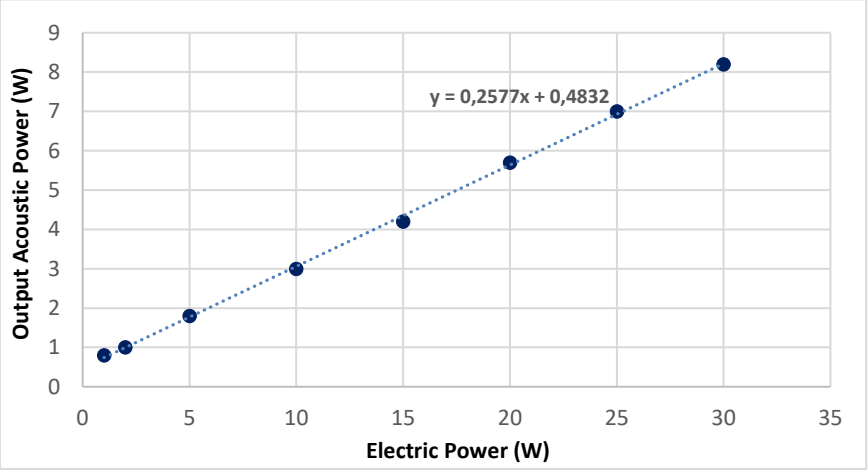

Figure 27: Acoustic versus electric power for the 1 MHz transducer.

2.75 MHz Transducer

The efficiency of the 2.75 MHz transducer was calculated using the same procedure as before. The power range used was 0-30 W, as per manufacturer instructions. The corresponding acoustic powers measured by the power meter are listed in Table 6. The first column shows the total electrical power sent from the amplifier to the transducer, while the second column shows the acoustic power produced.

Table 6: The electrical power applied, and acoustic power produced.

Electric Power (W)	Acoustic Power (W)
10	3.2
20	6.0
30	8.8

The efficiency of a transducer as calculated using equation [1] is equal to 28%. Figure 28 shows the measured acoustic power plotted against the applied electric power. The efficiency of the transducer as estimated by linear fitting is 28.7 %.

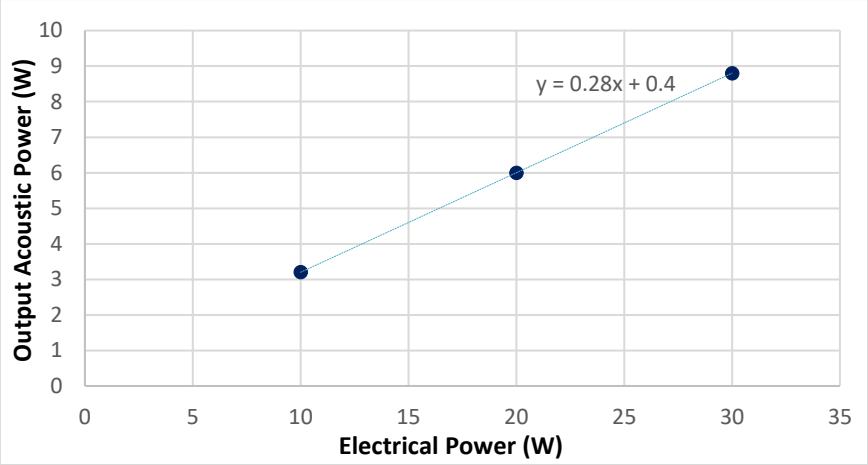

Figure 28: Acoustic versus electric power for the 2.75 MHz transducer.

Ultrasonic field measurements using hydrophone

The actual focal distance and approximate focal point length of the transducers were estimated by evaluating the axial power field. A dedicated 3D printed plastic holder was fixed within an acrylic tank filled with degassed water to accommodate the transducer (transmitter) and the hydrophone (PVDF-Z44-1000, Specialty Engineering Associates, Soquel, CA), which served as the signal receiver. The 3D printed holder provided the possibility of linear movement of the transducer in an axial direction. Figure 29 shows the CAD drawing of the experimental set-up.

The transducer was connected to the RF amplifier (AG1016, AG Series Amplifier, T & C Power Conversion, Inc., Rochester, US), which supplied it with 5 W of electrical power. A digital oscilloscope (TDS 2012, Tektronix, Inc., 14150 SW Karl Braun Drive, United States) was wired to the hydrophone to display the received signal. Figure 30 shows the experimental set-up that was used for the power field measurements.

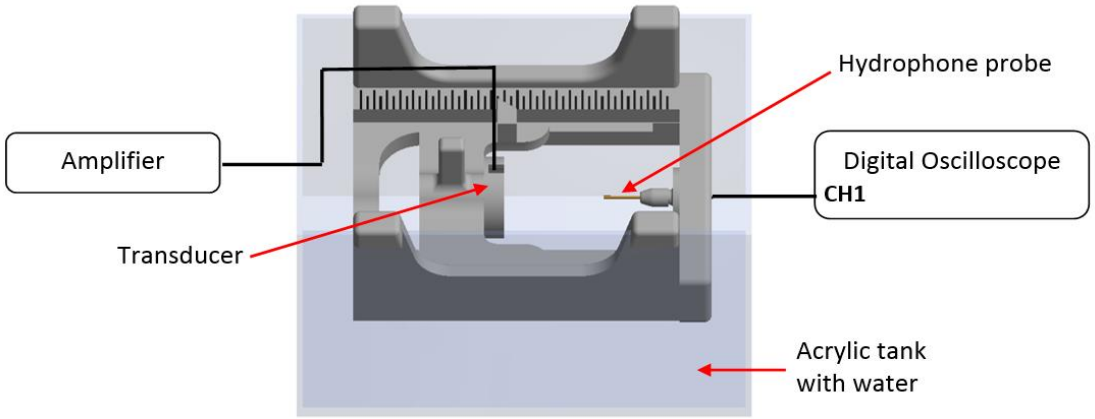

Figure 29: CAD drawing of the experimental set-up that was used for the power field measurements.

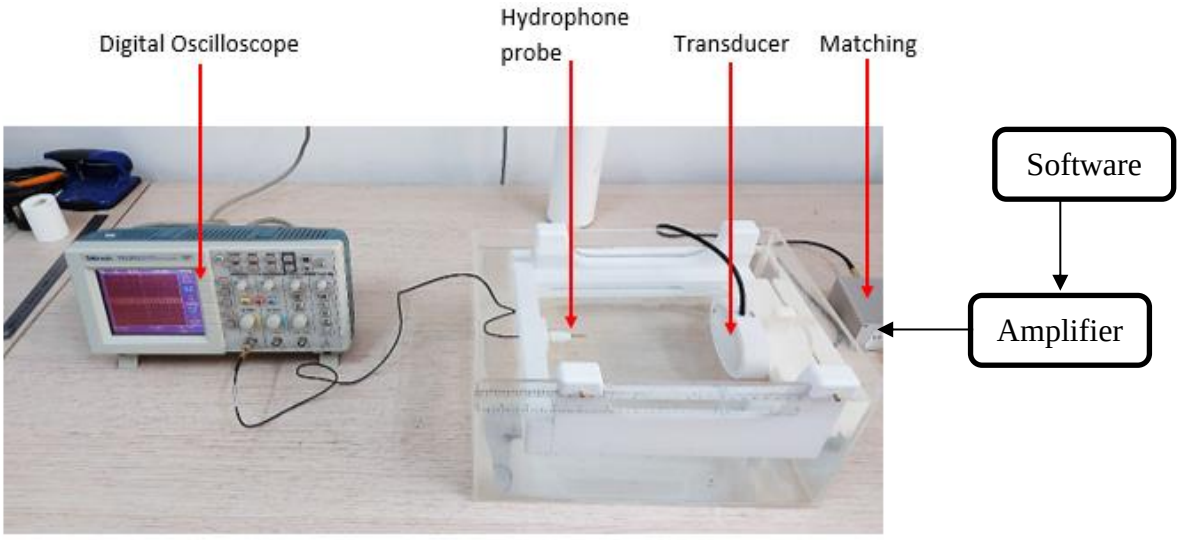

Figure 30: Experimental set-up that was used for the power field measurements.

1 MHz Transducer

The axial power field of the transducer with a frequency of 1 MHz was evaluated by measuring the peak-to-peak voltage at various distances between the transmitter (transducer) and the receiver (hydrophone). A power of 5 W was applied in each case. The distances tested were in the range of 1 to 14.5 cm from the transducer surface, with a measurement interval of 0.5 cm. Figure 31 shows the measured voltage plotted against the axial distance between the transducer and hydrophone.

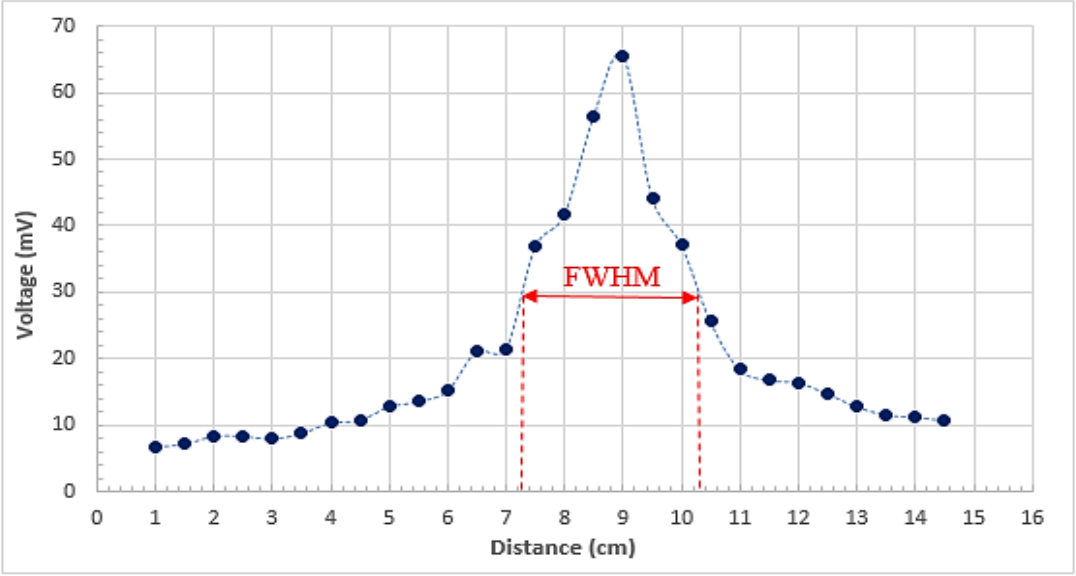

Figure 31: The voltage plotted against the axial distance from the transducer, for 5-mm interval measurements.

Referring to the graph of Figure 31, the actual focal length is at a distance of 9 cm from the surface of the transducer. The axial pressure profile approximately follows a gaussian distribution around the focal spot characterized by a FWHM of 30 mm.

2.75 MHz Transducer

The peak-to-peak voltage measurements for different transmitter-to-receiver axial distances were repeated for the transducer with a frequency of 2.75 MHz. The tested distances ranged from 1 to 14.5 cm and an electrical power of 5 W was applied in each case. Figure 32 shows the measured voltage plotted against the axial distance between the transducer and hydrophone.

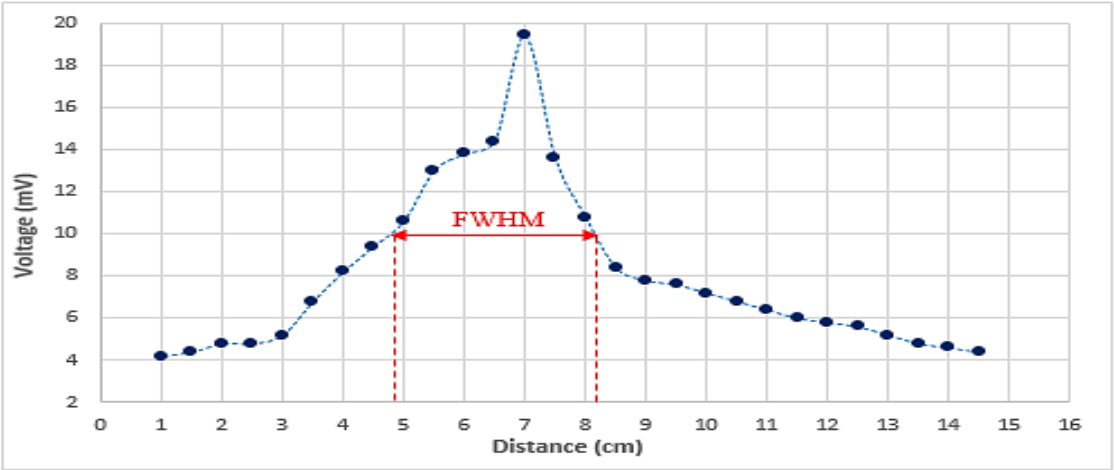

Figure 32: The voltage plotted against the axial distance from the transducer, for 5 mm interval measurements.

According to these results, the actual focal point of the 2.75 MHz transducer is located at a distance of 7 cm from the transducer surface. Assuming a gaussian axial distribution of pressure around the focal point, the FWHM is about 30 mm.

Ultrasonic field evaluation using transparent plastic films

Sonication of transparent plastic films (Stratasys FDM400mc print plate, thickness: 0.9 mm, dimensions: 55 mm x 55 mm) was performed to evaluate the acoustic field of the developed transducers (frequency: 1 MHz, diameter: 90 mm, radius of curvature: 100 mm and frequency: 2.75 MHz, diameter: 50 mm, radius of curvature: 65 mm). The efficiency of the 1 and 2.75 MHz transducers was estimated at 25.8 % and 28.7 %, respectively, using the previously described methodology. The transducer and the plastic film were fixed to a 3D printed plastic holder, which was placed in a water tank for proper acoustic coupling. The transducer was mounted at the bottom of the water tank facing towards the plastic film, so that the ultrasound beam is directed towards the center of the plastic film. The transducer's holder provided the ability to modify the transducer-film distance in 5- and 10-mm increments. The transducer was supplied by an RF amplifier (AG1016). An in-house developed dedicated software was used to control the ultrasound parameters (sonication power and time). The experimental method employed is based on the reflection of ultrasonic waves at the plastic/air interface. Therefore, it was important to set the water level at the bottom surface of the plastic film as well as to remove any air bubbles.

Figure 33 shows the experimental set-up used for the sonication of the plastic films and Figure 34 shows a schematic illustration of the concept of the experiment.

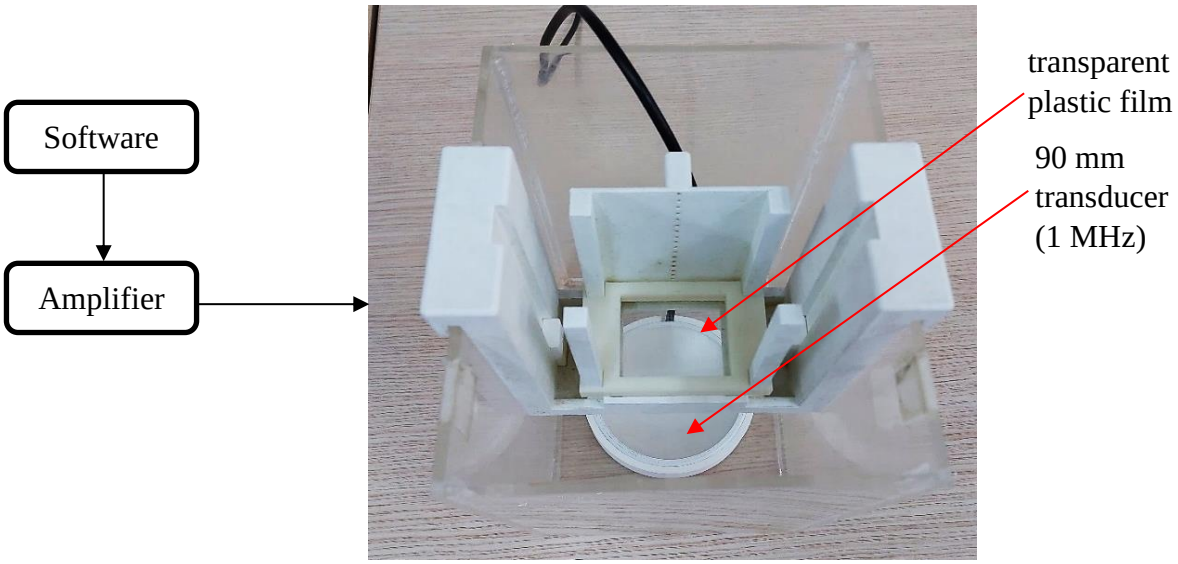

Figure 33: Experimental setup used to evaluate the acoustic field of the transducer on plastic films.

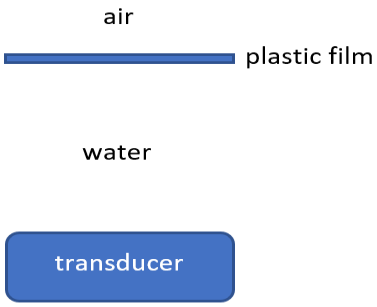

Figure 34: Concept of the experiment.

The effect of the distance between the film and the 1 MHz transducer on lesion formation and lesion dimensions was assessed. The sonication time and acoustic power remained at 30 s and 64.5 W, respectively, for all cases. Figure 35 shows the plastic films that were sonicated using acoustic power of 64.5 W (for 30 s) at different distances from the 1 MHz transducer. The maximum distance of the transducer from the plastic film surface at which lesion was created was 10 cm.

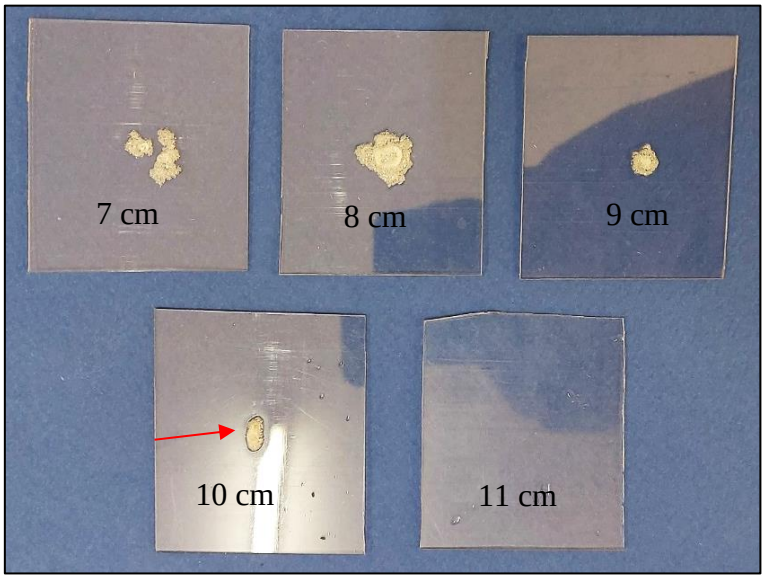

Figure 35: Plastic films sonicated at different distances from the 1 MHz transducer by applying acoustic power of 64.5 W (for 30 s).

Table 7 lists the dimensions of the lesions created on the plastic films for different distances of the 1 MHz transducer from the plastic film.

Table 7: List of dimensions of lesions formed on the plastic films using the 1 MHz transducer.

Plastic film	Electric power (W)	Acoustic power (W)	Energy (J)	Distance film/transducer (cm)	Lesion Formation (Y/N)	Area (mm^2)
1	250	64.5	1935	7	Y	11.2 x 11.5
2				8	Y	10.6 x 10.7
3				9	Y	5.2 x 5.8
4				10	Y	3.0 x 5.9
5				11	N	-

The ability of the higher frequency transducer (2.75 MHz) to form lesion at different distances form the plastic film was then investigated. The sonications were performed using an acoustic power of 42 W and a sonication time of 30 s. Figure 36 shows the plastic films that were sonicated at different distances from the 2.75 MHz transducer. Accordingly, Table 8 lists the dimensions of the lesions created on the plastic films for the tested distances.

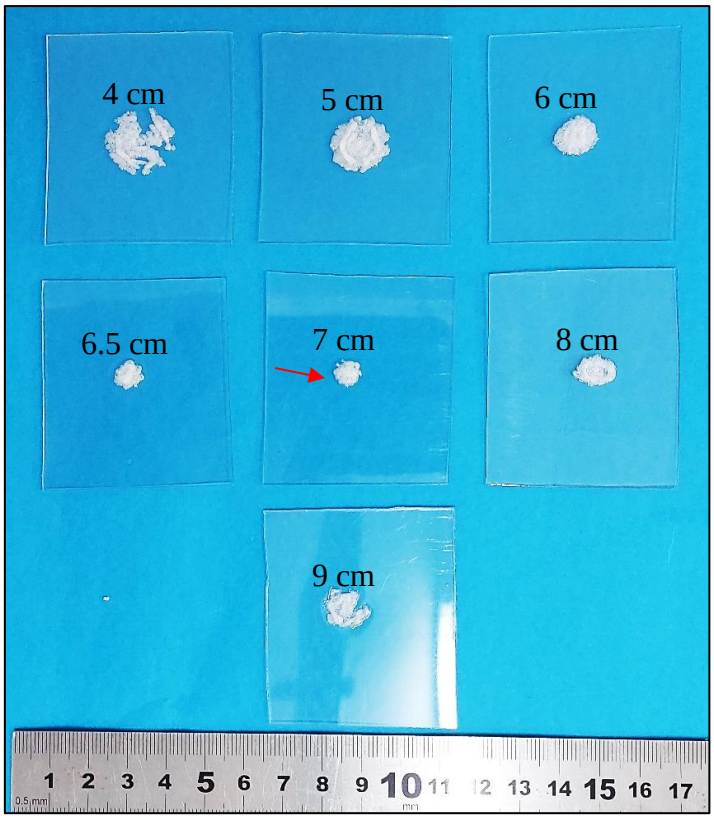

Figure 36: Plastic films sonicated at different distances from the 2.75 MHz transducer by applying acoustic power of 45 W (for 30 s).

Table 8: List of dimensions of the lesions formed on the plastic films using the 2.75 MHz transducer.

Plastic film	Electric power (W)	Acoustic power (W)	Energy (J)	Distance film/transducer (cm)	Destroyed area (Y/N)	Area (mm^2)
1	150	42	1350	4	Y	17.5 x 17.3
2				5	Y	15.1 x 14.6
3				6	Y	11.0 x 10.3
4				6.5	Y	7.2 x 7.5
5				7	Y	6.9 x 6.6
6				8	Y	10.9 x 7.8
7				9	Y	11.6 x 10.6

Conclusions

Two transducers were specially designed to be incorporated in the FUSVET robotic device. Both transducers were designed to be single element, spherically focused, MR compatible and compact. The selection of their structural characteristics was based on HIFU beam simulations of candidate transducers on the criterion of achieving strong focusing of ultrasonic waves over a large depth. Eventually, a transducer with a central frequency (f) of 2,75 MHz, a diameter (D) of 50 mm and a radius of curvature (R) of 65 mm was chosen for targeting shallow tissue. Since attenuation affects the ultrasonic beams of higher frequency to a greater degree (i.e., waves of higher frequencies undergo greater scattering) limiting the penetration depth, a smaller frequency of 1 MHz was selected for deeper-seated targets. Specifically, a transducer with a central frequency of 1 MHz, 90-mm diameter, and 100-mm radius of curvature was chosen.

The simulated HIFU beams produced strong thermal effects. For both simulated beams, sufficient amount of ultrasonic energy reached the simulated tissue resulting in the formation of ellipsoid lesions of well measurable dimensions by applying an acoustical power of 60 W for 30 s. Specifically, sonication with the 1 MHz transducer resulted in a temperature increase of 33.3 ºC at the focal depth of 1.77 cm. The accumulated thermal dose was sufficient to cause a thermal damage of about 9 mm in length and 1.8 mm in diameter. An identical sonication was performed using the 2.75 MHz transducer. The result was a temperature increase close to 100 ºC at a focal depth of 1.802 cm and a thermal lesion measuring 11.7 mm in length and 3.2 mm in width. As expected, higher ultrasonic intensities and temperatures were predicted for the 2.75 MHz beam due its stronger focusing (theoretically defined as cR/fD, where c is the speed of sound in the medium).

Purchased piezoelectric elements with the specific characteristics were hosted in custom-made housings made of ASA plastic and sealed with epoxy to create the transducers. The epoxy layer serves as the backing material isolating the electric contacts and preventing excessive vibration of the piezoelectric element, whilst simultaneously improving the acoustic performance of the transducer.

Maximum power transfer to the transducers was achieved by adjusting their impedance to 50 Ω. The efficiency (i.e., the percentage of applied electrical power converted to acoustic power) of the selected transducers was improved by creating and integrating the corresponding matching device. The achieved efficiency, as estimated by the radiation force balance method, is 25.8% and 28% for the transducers with frequencies of 1 and 2.75 MHz, respectively.

The materials and components utilized for manufacturing the ultrasonic transducers were specially chosen to achieve MRI compatibility. Furthermore, when in use in the MR environment, the transducer is connected to a specially designed low-pass RF filter for preventing image distortions effects. Notably, assessment of the transducers' compatibility with a 3T MRI scanner in terms of safely operating without affecting the quality of imaging significantly is the subject of deliverable 3.4.

The actual acoustic pressure distribution in the axial direction was estimated for both transducers using hydrophone-based measurements. The transducer was the transmitter, and a

hydrophone was used as the receiver. Regarding the 1 MHz transducer, the experiments revealed an actual focal distance of 9 cm. An effective focal distance of 7 cm was found for the 2.75 MHz transducer.

The ultrasonic field of the two spherically focused transducers (1 and 2.75 MHz) was further evaluated by sonicating transparent plastic films. The ultrasonic field of the 1 MHz transducer was investigated by performing single sonications with a constant acoustic power of 64.5 W and a sonication time of 30 s. The parameter that was varied was the transducer-to-film distance. The smallest area of destruction (lesion) was observed at a distance of 10 cm, coinciding with the theoretical focal distance of the transducer. The largest destroyed area was observed at a distance of 7 cm, while at a distance of 11 cm no damage was observed on the film. This change in lesion size with varying distance is indicative of the change in beam size, and accordingly the power field distribution. Regarding the 2.75 MHz transducer, the sonications were carried out using an acoustic power of 42 W (electrical power 150 W) and a sonication time of 30 s at a range of different distances from 4 to 9 cm. The largest destroyed area was observed at the distance of 4 cm and was gradually decreased until the focal point (7 cm), where the smallest lesion was observed, thus providing additional evidence of the actual focal distance. The damaged area then started to increase in size as the film was moved further away from the focal point (i.e., at distances of 8 and 9 cm).

The current results suggest that the manufactured transducers can efficiently reach and ablate both shallow and deep tissue. Experiments in the framework of Task 3.5 (Evaluation of hardware), which include the transducers' evaluation in *ex-vivo* and *in-vivo* tissue, will provide further data regarding the focal spot location and heating capabilities of the developed transducers, and how they are affected by the specific tissue characteristics, to verify that treatment can be safely and efficiently delivered to the targeted tissue.

References

[1] HITU simulator (2017), Available at: https://www.fda.gov/about-fda/cdrh-offices/hitu-simulator (Accessed: February 2023).

[2] Stratasys (1989), Available at: https://www.stratasys.com/resources/search/white-papers/fortus-360mc-400mc (Accessed: February 2023).

[3] Anatech Electronics (1990), Available at: https://www.anatechelectronics.com/ (Accessed: February 2023).

[4] LE LEIVRE.COM, Available at: https://leleivre.com/rf_lcmatch.html (Accessed: February 2023).

[5] Coil32, Available at: https://coil32.net/online-calculators/multilayer-coil-calculator.html (Accessed: February 2023)